KFA

KERNFORSCHUNGSANLAGE JÜLICH GmbH

640

Contributions for the 14th Biennial Conference on Carbon

Papers to be Read at the Conference in Pennsylvania State University, 25 - 29 June 1979

compiled by

W. Delle

JUl - Conf - 31
April 1979
ISSN 0344-5798

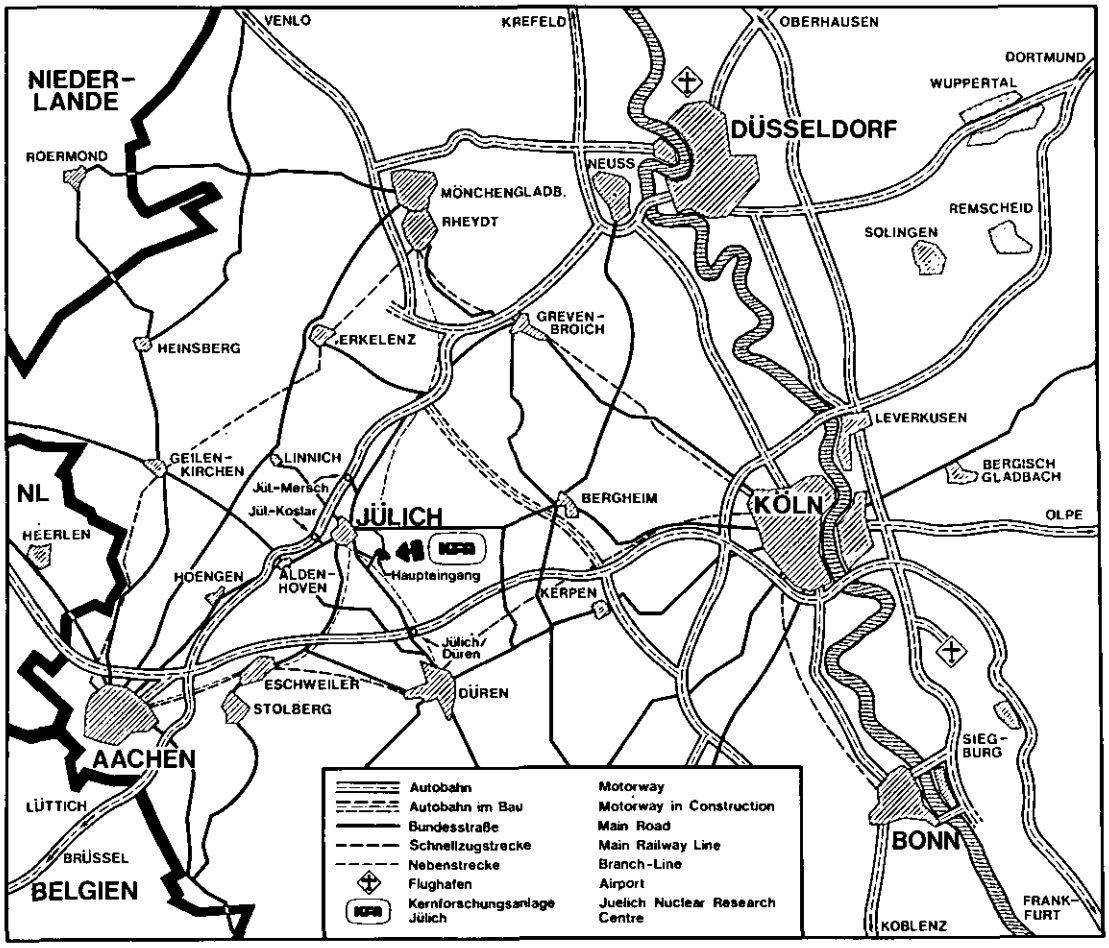

Als Manuskript gedruckt

Berichte der Kernforschungsanlage Jülich Jül - Conf - 31

Zu beziehen durch: ZENTRALBIBLIOTHEK der Kernforschungsanlage Jülich GmbH,
Jülich, Bundesrepublik Deutschland

Contributions for the 14th Biennial Conference on Carbon

Papers to be Read at the Conference in Pennsylvania State University, 25 - 29 June 1979

compiled by

W. Delle

List of Contributors

P. Ashworth
H. Cords
M. R. Cundy*
W. Delle
K. Frye
G. Haag
H. K. Hinssen
H. Hoven
M. Hrovat**
W. Katscher
G. Kleist
R. Moormann
H. Nickel
M. F. O'Connor
M. Rödig
R. J. Price***
F. Putsch
E. Wallura
R. Zimmermann

* J. R. C. EURATOM Petten, The Netherland
** HOBEG GmbH, Hanau, Fed. Rep. of Germany
*** General Atomic Company, San Diego, California (GAC)

CONTRIBUTIONS FOR THE 14TH BIENNIAL CONFERENCE ON CARBON JUNE 25TH - 29TH, 1979

COMPILED BY
W. DELLE

ABSTRACT

This report is the compilation of a number of papers prepared by KFA Jülich GmbH for the 14th Conference on Carbon which will be held in the Pennsylvania State University, 25-29 June, 1979. The presentations deal with results obtained from fast neutron irradiations, graphite and graphitic matrix corrosion experiments and characterization methods applied to nuclear graphite and fuel matrix.

The results described were partly achieved in the framework of the HTR Projects "Hochtemperaturreaktor-Brennstoffkreislauf" (High Temperature Reactor Fuel Cycle) and "Prototyp Nukleare Prozeßwärme" (Prototype Nuclear Heat) being financed from BMFT (Federal Ministry for Research and Technology) and the State of "Nordrhein-Westfalen".

Beiträge zur 14. Kohlenstoff-Konferenz vom 25. bis 29. Juni 1979

ZUSAMMENGESTELLT VON
W. Delle

Kurzfassung

Dieser Bericht enthält die Zusammenstellung von Beiträgen der KFA Jülich GmbH für die Kohlenstoff-Kohlenstoff-Konferenz, die in diesem Jahr vom 25. bis 29. Juni an der Pennsylvania State University stattfindet.
In den Vorträgen werden Ergebnisse von Materialbestrahlungen mit schnellen Neutronen, Korrosionsexperimenten, Werkstoffcharakterisierungen für Graphit und Kohlenstoff-Matrixmaterial behandelt.
Die in dem Bericht beschriebenen Ergebnisse entstanden zum Teil im Rahmen der HTR-Projekte "Hochtemperaturreaktor-Brennstoffkreislauf" und "Prototyp Nukleare Prozeßwärme", die vom Bundesministerium für Forschung und Technologie und vom Land Nordrhein-Westfalen gefördert werden.

Inhaltsverzeichnis Seite

Einleitung

In den USA finden jeweils im Abstand von zwei Jahren Kohlenstoff-Konferenzen statt, auf denen Wissenschaftler aus aller Welt ihre neusten Forschungs- und Entwicklungsergebnisse vorstellen und diskutieren können. Die Konferenz wird von der American Carbon Society und der Institution, an der die Konferenz jeweils stattfindet, getragen. Im Jahre 1979 wird dies die Pennsylvania State University sein.
Zwischen diesen Konferenzen finden abwechselnd in der Bundesrepublik Deutschland und Großbritannien entsprechende europäische internationale Konferenzen statt. Im Jahre 1978 war mit der Fifth London International Conference on Carbon and Graphite London der Austragungsort, für die 1980 stattfindende CARBON '80 wurde Baden-Baden zum dritten Male ausgewählt.

Für die 14. Carbon-Konferenz in Pennsylvania konnten Vorträge zu folgenden Gebieten angemeldet werden:
Mesophase, Verkokung, Graphitierung, chemische Reaktivität und Oberflächen, elektrische und thermische Eigenschaften, Anwendung als Biomaterialien, faserverstärkte Werkstoffe und ihre Anwendung, Kunstkohlenstoff und -graphit mit Anwendungen, nukleare Anwendungen, mechanische Eigenschaften und Reibung, Aktivkohle und Adsorption; Einlagerungsverbindungen und Kohlenstoffcharakterisierung.
Es wurden insgesamt 240 Vorträge angemeldet; 8 davon entstanden unter maßgeblicher Beteiligung der Kernforschungsanlage Jülich GmbH.

Die Vortragsveröffentlichungen der KFA-Beiträge sind in dem vorliegenden Bericht zusammengefaßt.

PROPERTY CHANGES IN GRAPHITE IRRADIATED AT CHANGING IRRADIATION TEMPERATURE

R.J. Price, General Atomic Company, San Diego, California 92138
G. Haag, Kernforschungsanlage Jülich GmbH, Federal Republic of Germany

Introduction

Standard irradiation tests for obtaining design data on graphite are carried out as nearly as possible at constant temperature, and the data are presented as families of isothermal plots showing the change in property as a function of fast neutron fluence. Such isothermal test data can be applied directly to the fuel element blocks in a base load power reactor, but in other systems graphite may be irradiated at widely varying temperatures. Large temperature fluctuations would occur in the fuel elements of a pebble bed HTR utilizing the OTTO cycle, a prismatic block HTGR operating with axial push-through, or a fission-fusion hybrid power system using a breed-burn cycle. Design calculations require a method for combining isothermal plots to predict accurately the property changes.

Rules for Combining Isothermal Curves

Simple empirical procedures have been suggested in the literature (Refs. 1,2) for transposing isothermal dimensional change curves. Figure 1 is a schematic plot illustrating three alternative empirical rules for accounting for the dimensional changes in a typical nuclear graphite irradiated first at 600°C, then at 1000°C. Figure 1(a) shows the complete isothermal dimensional change-versus-fluence plots for 600°C and 1000°C. Figures 1(b), 1(c), and 1(d) show three alternative ways of joining the 1000°C isotherm to the 600°C isotherm following a step change in temperature to 1000°C after a period of exposure at 600°C.

Rule 1, vertical transposition at equal fluence, [Figure 1(b)] is the simplest procedure. At the point of temperature change, the 1000°C isotherm is shifted vertically by an amount $(y_2 - y_1)$ to join the 600°C isotherm at the same fluence. Point (A) corresponds to point (x_1, y_2) on the isotherm. This procedure fails to predict changes in properties such as thermal conductivity which are controlled by a transient population of small defect clusters.

Rule 2, horizontal transposition at equal property value, is illustrated in Figure 1(c). At the temperature change point, the 1000°C isotherm is shifted horizontally a distance $(x_1 - x_2)$ to join the 600°C isotherm for the same dimensional change value. In this case, point (A) corresponds to point (x_2, y_1) on the isotherm. Rule 2 has some justification when applied to cumulative-type properties, such as high temperature dimensional change, if it is assumed that a given dimensional change corresponds to a given state of irradiation damage. The main drawback is that the procedure is sometimes mathematically impossible, as would be the case if the temperature change occurred near the minimum in the 600°C isotherm.

Rule 3, is proposed here here as a method which fits the fullest range of properties and fluence situations. It may be described as horizontal transposition at a scaled fluence, and is illustrated in Figure 1(d). The fluence accumulated at any irradiation temperature, T, is converted to a scaled fluence by dividing by the lifetime fluence, L(T). L(T) is taken to be the fluence where the dimensional change becomes positive [x_3 and x_4 in Figure 1(a)]. The 1000°C isotherm is shifted horizontally until point A (corresponding to a fluence of $x_1 \times x_3/x_4$ on the original isotherm) falls at a fluence of x_1. At this point the scaled fluence at 600°C equals the scaled fluence at 1000°C. Any gap between the two isotherms is progressively reduced according to the expression:

$$y = y^* + \Delta y \exp\left(-\frac{\gamma}{\tau}\right)$$

where y is the predicted property value, y^* is the property value on the transposed T_2 isotherm, Δy is the gap between the isotherms at the temperature change point, γ is the fluence measured from the temperature change point, and τ is a time constant whose value is taken to be 1×10^{21} n/cm^2 (equivalent fission fluence for graphite damage).

Comparison With Experimental Data

Experimental data from several programs in which the irradiation temperature of graphite specimens was systematically changed have been reviewed. Measurements of changes in dimensions, Young's modulus, thermal conductivity and thermal expansivity were considered. Examples are shown in Figures 2 and 3. Overall, the measurements agree well with predictions based on the third transposition rule, whereas the first and second rules sometimes give rise to false predictions or no predictions at all.

Acknowledgements

This report was prepared under the Umbrella Agreement for cooperation in Gas-Cooled Reactor Development between the United States and the Federal Republic of Germany. The work was supported by the U.S. Department of Energy and partners in the Hochtemperaturreaktor-Brennstoffkreislauf Project.

References

1. Engle, G.B., USAEC Report Gulf-GA-A12080 (1972).

2. Delle, W.W., et al., Abstracts of the 11th Biennial Conference on Carbon, Gatlinberg (CONF-730601), p. 300 (1973).

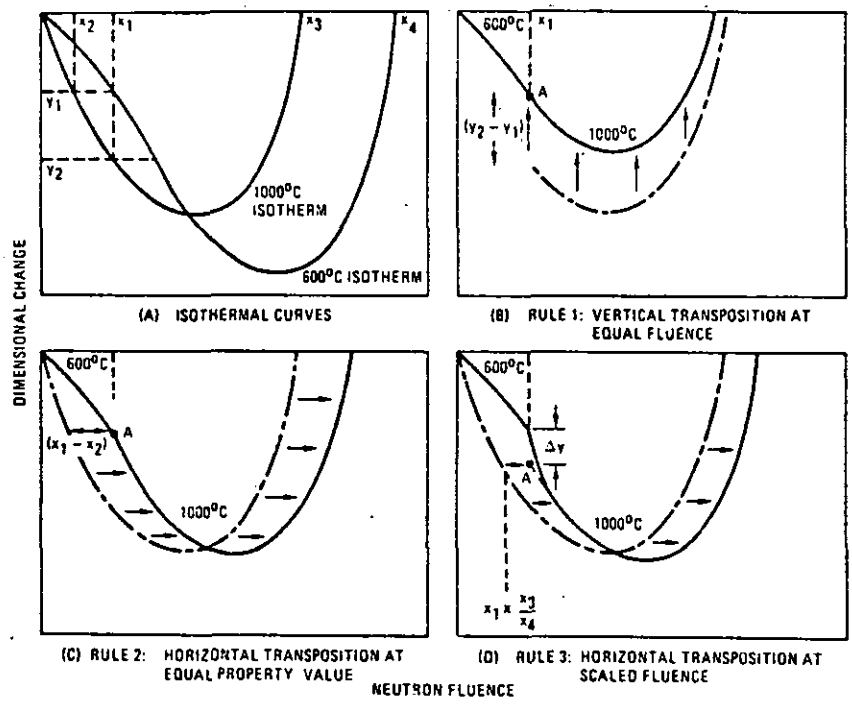

Figure 1. Alternative Rules for Transposing Isothermal Plots of Graphite Dimensional Change Versus Fluence

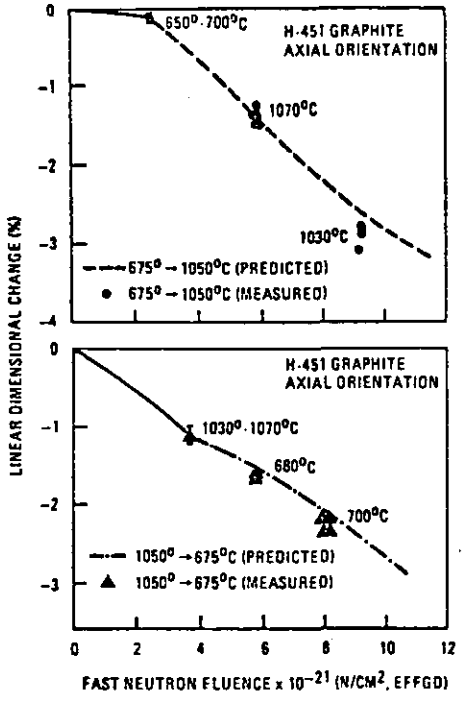

Figure 2. Irradiation-Induced Changes in H-451 Graphite, Axial Direction, with Changing Temperature

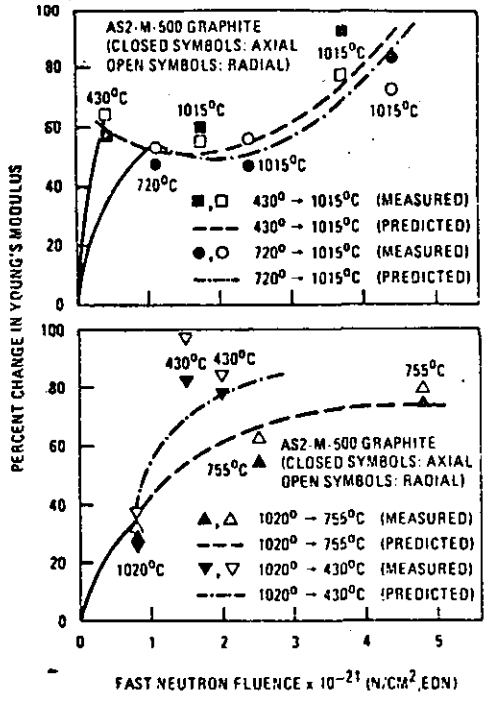

Figure 3. Irradiation-Induced Changes in Young's Modulus of AS2-M-500 Graphite, with Changing Temperature

HIGH FLUENCE GRAPHITE CREEP EXPERIMENTS RELEVANT FOR THE PEBBLE BED HTR

G. Kleist*, M. F. O'Connor**, M. R. Cundy**
*Kernforschungsanlage Jülich GmbH
D-5170 Jülich
Federal Republic of Germany
**EURATOM Joint Research Center
Petten
The Netherlands

General scope of the creep investigations

The pebble bed High Temperature Reactor (HTR) of the OTTO-type (Once Through Then Out - refering to the pebble fuel elements) which is being developed in the Federal Republic of Germany, has a graphite reflector which in the course of reactor life will be subjected to very high neutron fluences in excess of 3×10^{22} cm^{-2} (DNE) in the temperature range 300 to 750 °C. The highly exposed regions are the upper side and top reflector. Substantial qualification work and irradiation testing is being carried out in the Petten High Flux Reactor (HFR) and the Oak Ridge High Flux Isotope Reactor (HFIR) in cooperation with the Kernforschungsanlage Jülich. The maximum fluence reached to the end of 1978 with several candidate reflector graphites was 1.4×10^{22} cm^{-2} (DNE).

An undispensable part of irradiation testing is the investigation of the radiation creep behaviour of graphite up to those very high fluences where no creep data are as yet available. However, an extrapolation formula for the steady state creep coefficient has been proposed (1) which takes into account the structural changes of graphite during irradiation in terms of Young's modulus changes. According to this the creep coefficient K^* in the low fluence region up to 3×10^{21} cm^{-2} (DNE) is to be multiplied by a "structural factor" $S = E^*/E(\Gamma)$ in order to calculate the creep coefficient $K(\Gamma)$ at higher fluences

$$K(\Gamma) = K^* \cdot S = K^* \frac{E^*}{E(\Gamma)},$$

where $E(\Gamma)$ is the actual value of Young's modulus at fluence Γ and E^* is the plateau value at low fluence.

If this applies, the creep coefficient decreases from a constant value in the fluence interval 0.5 to 3×10^{21} cm^{-2} (DNE) up to about the point of maximum densification and thereafter can be expected to increase again. At present, irradiation creep tests are being carried out in the HFR Petten at 300 °C and 500 °C under tensile and at 500 °C also compressive stresses of 5 MPa + 2 % respectively with a maximum fluence of nearly 5.5×10^{21} cm^{-2} (DNE). By the end of this year a fluence of approximately 1×10^{22} cm^{-2}(DNE) will have been achieved. Another important value to be measured is Poisson's ratio in creep, of which not much information is available. Furthermore, the creep data from this programme will resolve possible differences in tensile and compressive creep behaviour in the high fluence region. In stress calculations of reflector blocks creep coefficients for tension and compression are generally assumed to be equal. This is, of course, rather convenient but seems to be an approximation (2).

Since the creep specimens are alligned in our irradiation rig in strings with axial fast flux profiles in the range 1.6 to 2.4×10^{14} cm^{-2}s^{-1}, some information on eventual fast flux dependence of the creep coefficient, proposed by Veringa and Blackstone (3) could be expected in our experiments. It must be said here, however, that indications for fast flux effect which were found only in the case of tensile creep (4) now proved to be statistically unsignificant on the 95 % confidence level on the basis of our new additional data.

Details of the irradiation device and the specimen geometries are to be found elsewhere (4). The graphite tested is an extruded semiisotropic pitch coke graphite, ATR-2E, from the company SIGRI Elektrographit GmbH which was one of the first available graphite grades of six being considered for possible use as material for the highly exposed pebble bed HTR reflector. Table 1 summarizes some typical preirradiation data for the second production lot of ATR-2E (∥,⊥: directions parallel or transverse to extrusion). Material from this lot was used in the experiments.

Apparent density/gcm^{-3}		1.74
Young's modulus/GPa (sonic measurement)	∥	8.55
	⊥	7.40
Tensile strength/MPa	∥	10.80
	⊥	9.05
CTE (20 - 500 °C)/10^{-6} K	∥	4.40
	⊥	4.95
Anisotropy factor (CTE)		1.12

Table 1: Typical properties of ATR-2E graphite

Results

Creep deformations and Wigner shrinkages of the stressed creep specimens and the unstressed reference specimens were measured out of pile in specially designed measuring equipment (4). Irradiation was interrupted after fluences of 0.5, 2.2 and 5.5×10^{21} cm^{-2} (DNE). Unfortunately, three tensile creep specimens at 300 °C and at 500 °C respectively were broken during rig handling and had to be replaced which meant that the available higher fluence results for creep in tension was limited.

The creep strains for every individual pair of creep and reference specimens are presented in Figures 1a-c. They have been corrected for elastic modulus changes caused by irradiation, but not for CTE changes due to creep strain.

From own results of an earlier creep programme (5) and from data found in literature (2, 6), it is estimated that the creep strains of Figures 1a-c in both the tensile and compressive modes would be reduced by less than 5 % if CTE corrections were applied, resulting in a reduction of the quoted creep coefficients by nearly the same percentage, under the assumption that the creep induced CTE changes are linear with creep strain. The precise CTE changes of the creep specimens due to creep strain will be measured at the end of the programme.

Mean steady state creep coefficients, $\bar{K}_2$ and $\bar{K}_3$, are derived separately for the second and third irradiation periods. They are quoted in each figure. There is a general tendency towards reduction of the creep coefficient at higher fluences in all Figures 1a-c. This is most significant for compressive creep at 500 °C since here more data are available than for the tensile modes at 300 °C and 500 °C. In Fig. 1a the mean creep coefficient $\bar{K}_3$ for the third (the last) irradiation step is based on three intact creep specimens, and in Fig. 1b even on only two specimens.

The structural factor S as a function of fast fluence would suggest a slower decrease of the creep coefficient than is observed.

Apart from this, a smaller creep coefficient results from compressive creep as compared to tensile creep at 500 °C with special reference to $\bar{K}_2$. The ratio of compressive to tensile creep coefficient is 0.77. The slightly larger creep coefficient (by 15 %) in tension at 300 °C as compared to 500 °C must not be significant although in one case such a tendency has been reported (7).

Acknowledgement

This work is being conducted within the frame work of the project "Hochtemperaturreaktor-Brennstoffkreislauf (High Temperature Reactor Fuel Cycle) which contains the partners Gelsenberg AG, GHT GmbH, Hobeg mbH, HRB mbH, KFA GmbH, Nukem GmbH, Sigri GmbH, Ringsdorff-Werke GmbH, and is financed by the Federal Ministry for Research and Technology and the state of Northrhine-Westfalia.

References

(1) *B.T. Kelly, J.E. Brocklehurst: Proc. Third Conf. Industr. Carbons Graphites. Soc. Chem. Indus. p. 363 (1971), London.*

(2) *J.E. Brocklehurst, R.G. Brown: Carbon 7, p. 487 (1969).*

(3) *H.J. Veringa, R. Blackstone: Carbon 14, p. 279 (1976).*

(4) *M.R. Cundy, G. Kleist, M.F. O'Connor, G. Pott: Proc. Fifth London Int. Carbon Graphite Conf. Vol. II, p. 959 (1978).*

(5) *G. Jouquet, M. Masson, R. Schill, G. Kleist, D.F. Leushacke, H. Schuster: High Temperature - High Pressures 9, p. 151 (1977).*

(6) *C.R. Kennedy, W.H. Cook, W.P. Eatherly: Proc. 13th Biennial Conf. on Carbon, Irvine Cal. p. 342 (1977).*

(7) *C.R. Kennedy: ORNL Annual Progr. Rep. 4170, p. 204 (1967).*

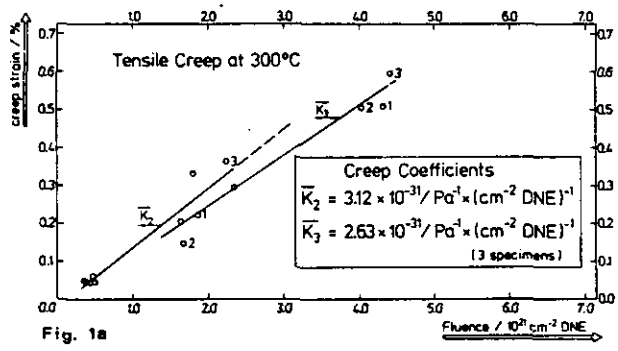

Fig. 1a

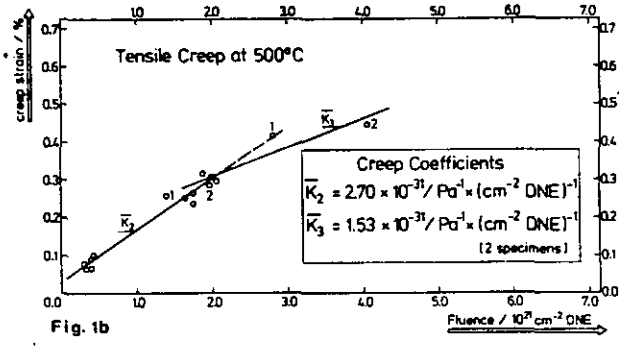

Fig. 1b

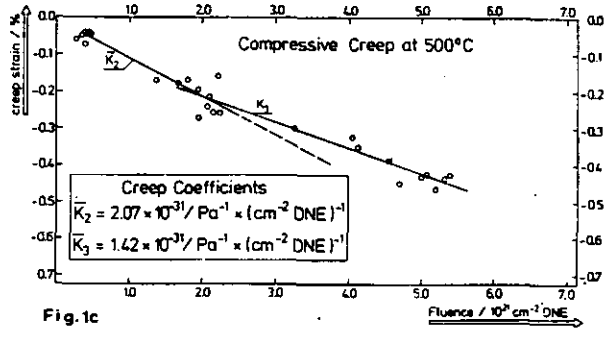

Fig. 1c

Figures 1a - c: Creep strain versus fast fluence at a stress of 5 MPa for graphite ATR-2E.
Mean creep coefficients are derived for two irradiation intervals.

MODEL ANALYSIS OF IRRADIATION-INDUCED CREEP EXPERIMENTS

H. Cords, R. Zimmermann, G. Kleist

Kernforschungsanlage Jülich GmbH, W.-Germany

Introduction

A semi-empirical model for irradiation induced changes in the material properties of graphite was described in refs. 2, 3) and its applicability was demonstrated for properties such as dimensional changes, Young's modulus, coefficient of thermal expansion and thermal conductivity. The model is based on the assumption that there are principally three saturating, atomic processes involved which influence the macroscopic properties by a linear relationship if there is no simultaneous closure of microcracks. The model can be interpreted to reproduce the so-called concept of equivalent temperatures, viz ref. 4). The present publication is in support of the earlier work to show that the creep behaviour is also governed by the fore-mentioned processes.

The Creep Coefficient as a Function of Temperature

Irradiation induced creep strains for graphite are considered to be proportional to the applied stress σ as well as proportional to the accumulated fast dose D. Furthermore, the creep coefficient $\varkappa$ i. e. the creep strain for unit dose and unit stress, was found to be less dependent on the type of graphite if multiplied by the appropriate Young's modulus E. Fig. 1 shows the measured creep coefficients for various graphites as a function of temperature. The data are usually fitted with an exponential function for temperatures above 500 °C, and they are considered to be constant for temperatures lower than this, viz ref. 6). The model fits, using the physical constants derived in ref. 3) and the importance factors α_2/E = 26,11 and α_2/E = 23,61 obtained from a fitting procedure, can account equally well for both the lower and the upper temperature region.

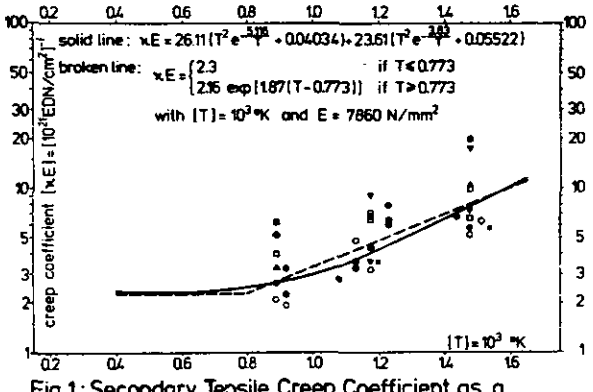

Fig.1: Secondary Tensile Creep Coefficient as a Function of Temperature from Ref[1] and Model Fits

Analysis for Creep Responses

For the purpose of analyzing the measured creep strains from ref. 5), the formula (22) from ref. 3) had to be extended to include an arbitrary number of step-changes, n, in the irradiation conditions and also to include the influence of the stress and flux density.

$$\varkappa = \sum_{i=2}^{3} S_i \alpha_i \sum_{j=1}^{n} \frac{\sigma_j}{E} u_j \alpha_{iD}(T_j\ D_j - D_{j-1}) \qquad (1)$$

with

$$u_j = u_{j-1}[1-\alpha_{iD}(T_{j-1}, D_{j-1})] - [\alpha_{iT}(T_{j-1}, \Phi_{j-1}) - \alpha_{iT}(T_j\ \Phi_j)]$$

and

$$D_{-1} = D_0 = T_0 = \Phi_0 = u_0 = 0\ ,\ D_n = D\ ,\ S_i = 1$$

All other symbols are explained in ref. 3) which also includes the flux dependency (eq. (17)). Eq. (1) only applies to the secondary creep component. The primary creep strain is recoverable, which requires that the elastic strains σ_j/E , are not applied to u_j as shown in equation (1). Instead the elastic strains are multiplied by the function α_{1T} . Also, it was found that by using

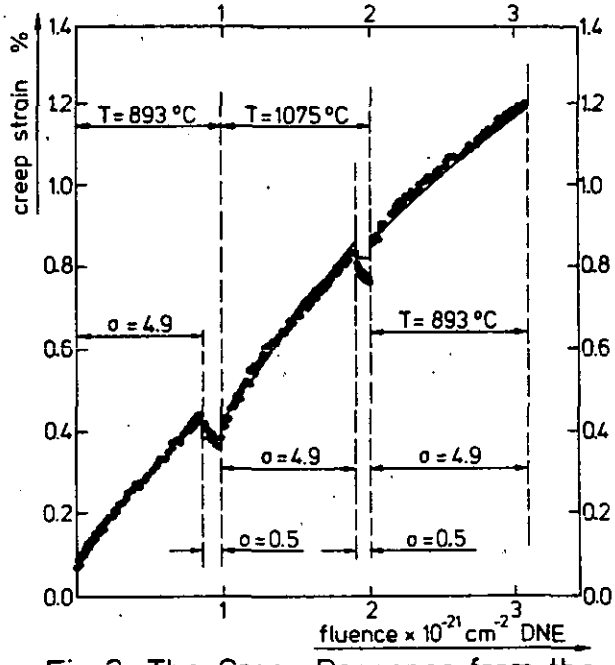

Fig. 2 : The Creep Response from the Experiment FLACH 03

Stress Units : MN/m^2

a dose dependent Young's modulus for calculation of the primary creep strains the fits were improved. The amount of the recovered primary strain was modelled by an additional, phenomenological parameter S. Using the four, free parameters S and σ_i with i = 1, 2, 3, there was no difficulty in fitting the creep strains of each of the four experiments from ref. 5). As an example, the result for the FLACH 03-experiment is shown in fig. 2.

Having established a set of importance factors, the model should be capable of predicting values for the creep coefficient with respect to temperatures and doses other than those at which the experiments were performed. For instance, it should be possible to reproduce the temperature dependence of the creep coefficient as shown in fig. 1 by using only the importance factors α_2 and α_3 from the analysis of the creep responses. As a result fig. 3 shows that the model predicts a creep coefficient which is in general slightly lower for lower temperatures and higher for higher temperatures if compared with measured data, which are smoothed results from restrained shrinkage experiments, viz broken line in fig. 1.

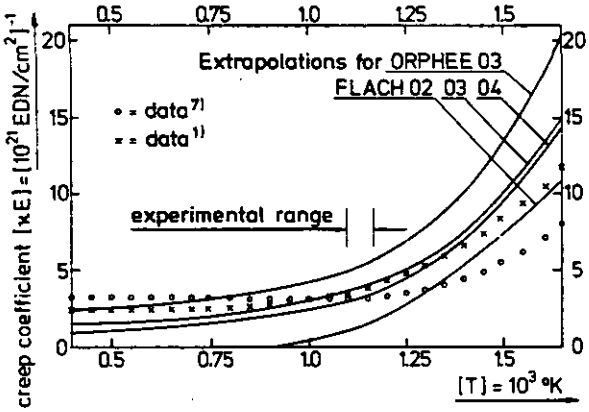

Fig.3: Secondary Tensile Creep Coefficient from Creep Characteristics

The Creep Coefficient as a Function of Dose

According to eq. (1), the creep strains for secondary creep are only in the initial stages directly proportional to the dose. For large values in dose the extrapolations seem to indicate a decrease in the creep coefficient. However, either due to a different characteristic behaviour for each graphite or simply due to a large scatter in the initial stage of irradiation, no unique solution for doses up to 30 x 10^{21} EDN/cm^2 has been found. The extrapolations on the basis of the FLACH 02-experiment had to be omitted from fig. 4 on the grounds that negative strains are unacceptable (see also fig. 3). There was also one case not depicted in fig. 4 which showed a characteristic behaviour with an initial decrease of the creep coefficient followed by an increase at higher doses. This type of curve would support the statement that the change in the coefficient for Secondary Creep as a function of dose depends predominantly on the irradiation induced changes of Young's modulus as far as these can be correlated to structural changes of the material, viz ref. 6).

Conclusions

The model is well capable of describing the creep response for low irradiation doses and accounts for the temperature dependence of the secondary creep coefficient. For the purpose of extrapolating a local solution to a wider range of irradiation temperatures and doses, the inherent scatter of the measured data seems to increase thus making the predictions uncertain. It is possible that the information necessary to forecast the full dose history is initially covered by other effects such as closure of microcracks, and irradiation induced shrinkage which contributes to the scatter of the measured strains.

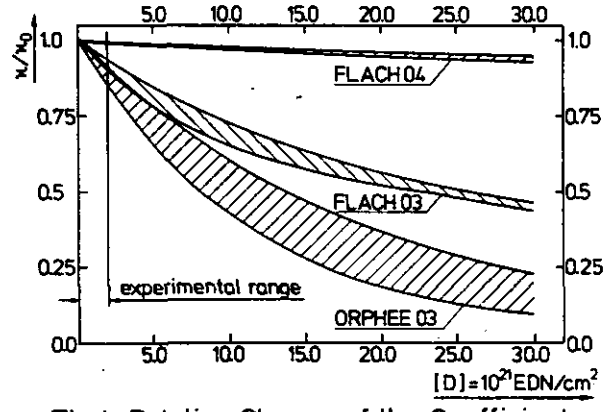

Fig.4: Relative Change of the Coefficient for Secondary Creep as a Function of Dose

References

1. Dragon Project Report No. 655, Fig. 12

2. H. Cords, R. Zimmermann - Proceedings of the 5th London International Carbon and Graphite Conference, London, Sept. 1978, p. 918

3. H. Cords, R. Zimmermann - Report of Kernforschungsanlage Jülich GmbH, JOL-1506, June '78

4. J. W. H. Simmons - Radiation Damage in Graphite. Pergamon Press, Oxford 1965

5. G. Jouquet, M. Masson, R. Schill, G. Kleist, D. F. Leushacke, H. Schuster - High Temperatures - High Pressures 9 (1977) 151

6. B. T. Kelly and J. E. Brocklehurst - Proc. 3rd Conference on Industrial Carbon and Graphite, Society of Chemical Industry, London, 1971, p. 363

7. G. Kleist - Internal Publication, KFA-IRW-TN-56/78

IRRADIATION BEHAVIOUR OF THE MATRIX A3-ISO 3 FOR THE PRISMATIC MONOLITHIC FUEL ELEMENT

W. Delle[+], G. Kleist[+], G. Haag[+], F. Putsch[+], M. Hrovat[++]

[+]Kernforschungsanlage Jülich GmbH, P.B. 1913, D 5170 Jülich

[++]HOBEG mbH, D 645 Hanau 11, Fed. Rep. of Germany

Introduction

The so-called monolith is a moulded block consisting of a substantially isotropic highly crystalline graphite matrix, fuel regions with the same matrix and cooling channels. The fuel zones contain spherical fuel particles coated with pyrolytic carbon and silicon carbide which are embedded in the graphite matrix. It is essential that the fuel regions are well bonded to the fuel free zone without any gap thus forming a continuous monolithic structure. The whole fuel element including fuel zones and cooling channels is manufactured only by moulding without any machining.

The monolith is fabricated in two steps applying a combined cold and hot moulding process. In the first step 64 wt.% natural graphite and 16 wt.% graphitized petroleum coke powder are wet mixed with 20 wt.% phenolformaldehyde resin and then dried. The resinated graphite matrix powder obtained is isostatically pressed to spheres under high forming pressure in a rubber die at room temperature in order to obtain an isotropic structure. The graphite spheres are then crushed to granules of 0.2-3 mm in size. In the second step the granulated graphite material is premoulded to a block in a steel die at room-temperature. After assembling the fuel rods into the fuel channels, the entire block together with the tool is heated to 180°C and moulded again. The heat treatments consist of two stages: The first works up to 800°C in order to carbonize the resin in an argon purge flow. In the second stage the block ist degassed in vacuum at temperatures up to 1,800°C (1). Complete moulded blocks including fuel as well as graphite matrix samples have been irradiated. In this paper only the results from irradiation experiments with the graphite matrix A3-Iso 3 are reported.

Experimental Method

35 matrix samples 10x10x25 mm^3 in size were irradiated in the HFR Petten/The Netherlands at temperatures between 400°C and 1,400°C in the frame of the joint DRAGON/ECN/EURATOM/KFA irradiation programme. Another irradiation test programme with this material was carried out in the FRJ-1 (MERLIN) Jülich at 500°C and 1,000°C in the fluence region below 10^{21} cm^{-2}EDN. A substantial part of additional work consisted in strength testing of about 240 irradiated and 70 unirradiated specimens of 9 mm length and 9 mm diameter by means of the diametrical compression test (2). In addition, 16 companion specimens of the same diameter but of 40 mm length were irradiated in order to obtain the irradiation induced changes of dimensions, electrical resistivity, ϱ, Young's modulus, E, and coefficient of thermal expansion (CTE), α. Fig. 1 shows the principle of the compression test. Perpendicular to the externally applied load, tensile stresses are induced in the sample, which finally lead to rupture. The rupture stress σ_c is calculated according to equ. (1).

$$\sigma = \frac{2 F_R}{DL \pi} \qquad (1)$$

where F_R is the rupture load and D and L are the diameter and the length of the specimen, respectively. The mean value of σ_c, in the case of the unirradiated samples, was related to the mean uniaxial ultimate tensile strength, $\overline{UTS}$, by a conversion factor:

$$\sigma_c = 0.8\ \overline{UTS} \qquad (2)$$

Results

Fig. 2 shows the fluence dependent dimensional change of samples irradiated in the HFR at different temperatures. The dimensions are changed anisotropicly due to the pre-irradiation anisotropy, ratio, $A = \alpha_{\perp} / \alpha_{\parallel}$ of 1.6, especially at temperatures higher than 1,000°C. The anisotropic irradiation behaviour was turned out to be smaller in fuelled blocks which were produced later and irradiated in the DRAGON Reactor. Fig. 5 demonstrates the increase in CTE which is larger than in normal graphites. Fig. 6 shows the CTE changes in the fluence region below 10^{21} cm^{-2}EDN from the irradiations at low fast neutron flux in the FRJ-1.

It becomes obvious that the curves for the changes in CTE are not as smooth as generally demonstrated in figures basing on accelerated irradiation tests.

Fig. 3 and fig. 4 show the irradiation induced increase of Young's modulus and strength as derived from the diametrical compression test at irradiation temperatures of 500°C and 1.000°C. The modified LOSTY and ORCHARD relation (3) between Young's modulus and strength (suffices 0 before and irr. after irradiation)

$$\frac{\overline{\sigma}_{c,\,irr.}}{\overline{\sigma}_{c,\,o}} = K \cdot \sqrt{\frac{\overline{E}_{irr.}}{\overline{E}_{o}}} \qquad (3)$$

applies with K = 0.93 for the irradiation temperature of 500°C and K = 1 for 1,000°C. The mean values $\sigma_{c,irr.}$ and $E_{irr.}$ are due to a fluence of 4×10^{20} cm^{-2}EDN.

The increase in electrical resistivity was found to be dependent upon irradiation temperature and pre-irradiation value: The lower the pre-irradiation value and the higher the irradiation temperature the smaller is the fractional increase. The decrease in thermal conductivity as estimated from increase of electrical resistivity was nearly 70% at the irradiation temperature of 500°C and after a fluence of 0.8×10^{21} cm^{-2}EDN.

References

1. Hrovat, M., Rachor, L., Huschka, H.: European Nucl. Conf., Paris 1975, G 2-Fuel Fabrication
2. Carneiro, F.L.L., Barcallos, A., Bull. RILEM, March 1955
3. Losty, H.H.W., Orchard, J.S.: Proc. 5th Conf. Carbon, 1962

Acknowledgements

This work has been carried out in the framework of the Project "Hochtemperaturreaktor-Brennstoffkreislauf" (High Temperature Reactor Fuel Cycle) that includes the partners Gelsenberg AG, Gesellschaft für Hochtemperaturreaktor-Technik mbH, Hochtemperaturreaktor-Brennelement GmbH, Hochtemperatur-Reaktorbau GmbH, Kernforschungsanlage

Jülich GmbH, Nukem GmbH, Sigri Elektrographit GmbH, Ringsdorff-Werke GmbH and is financed from BMFT (Federal Ministry for Research and Technology) and the State of Nordrhein-Westfalen.

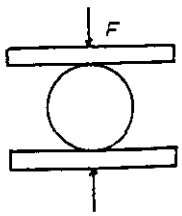

Fig. 1: Scheme of the diametrical compression test

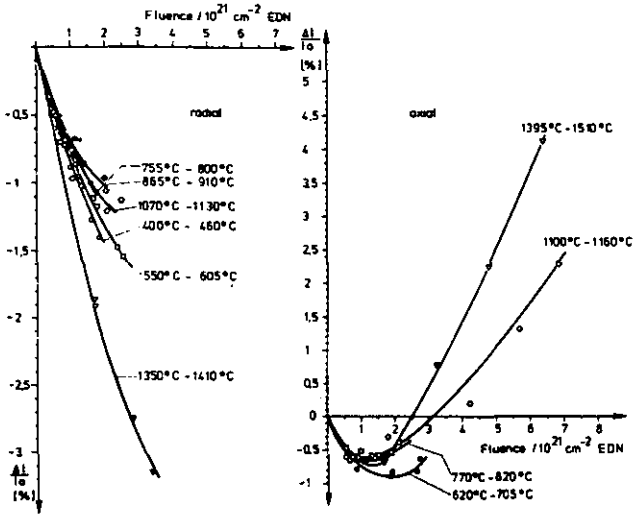

Fig. 2: Dimensional change versus fluence for different irradiation temperatures

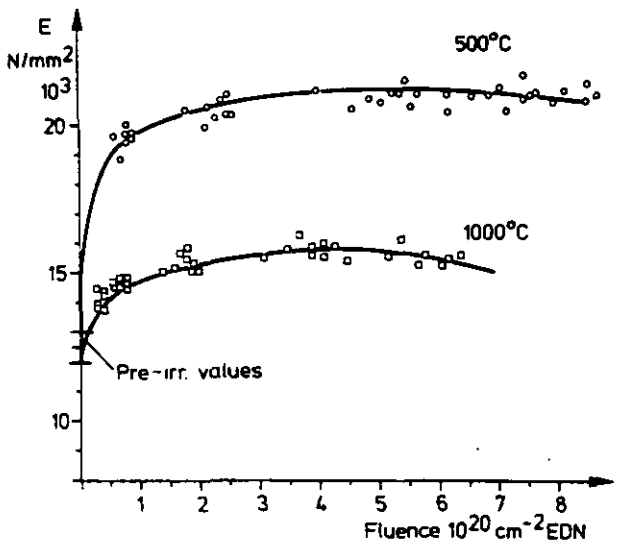

Fig. 3: Change in Young's modulus versus fluence at irradiation temperatures of 500°C and 1000°C

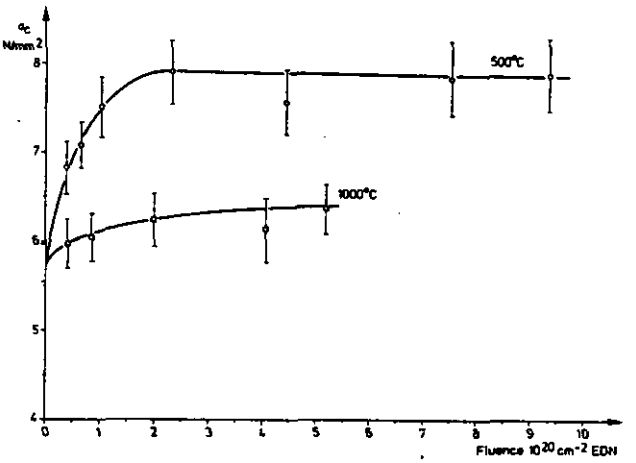

Fig. 4: Strength of diametrical compression versus fluence at irradiation temperatures of 500°C and 1000°C

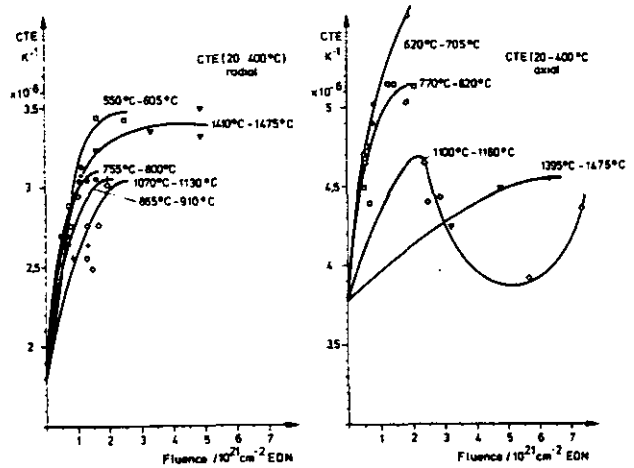

Fig. 5: Change in CTE versus fluence for different irradiation temperatures

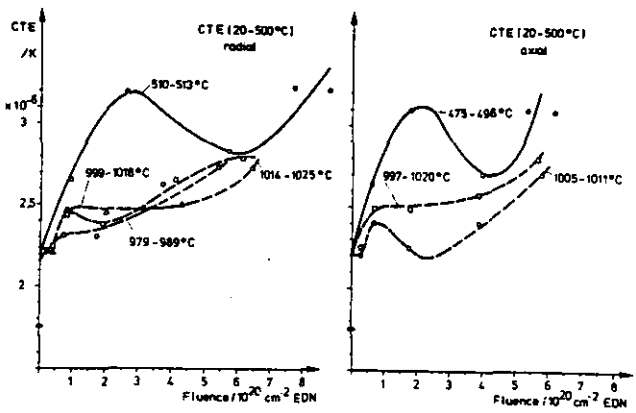

Fig. 6: Change in CTE versus fluence at irradiation temperatures of 500°C and 1000°C

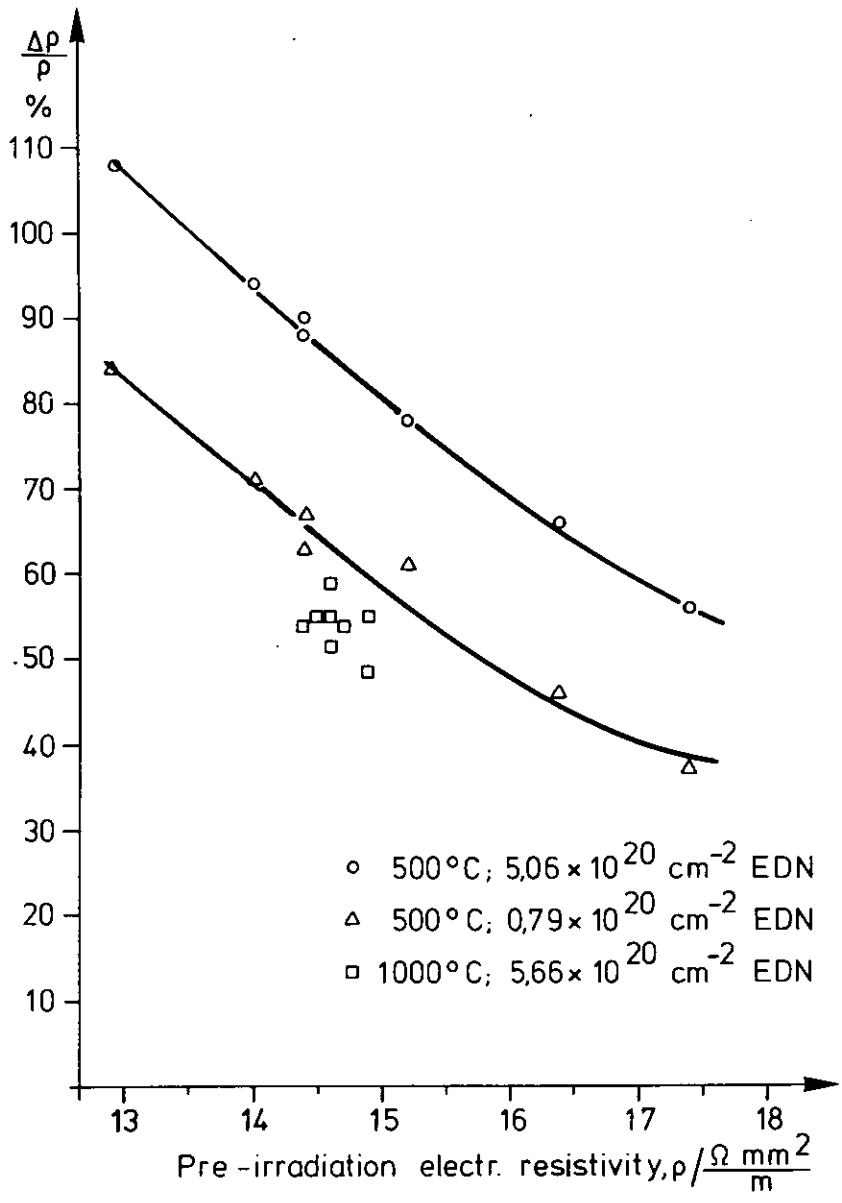

Fig. 7: Irradiation induced fractional change of electrical resistivity, $\Delta\varrho/\varrho$, versus pre-irradiation electrical resistivity, ϱ . Irradiation temperatures: 500°C and 1000°C.

FAST NEUTRON INDUCED CHANGES IN POROSITY OF GRAPHITIC MATERIALS

W. Delle, H. Hoven, K. Frye, E. Wallura, H. Nickel
Kernforschungsanlage Jülich GmbH, P.B. 1913, D-517 Jülich, Federal Republic of Germany

Introduction

During the fabrication of graphite materials both macro- and micropores are formed. Macropores are derived from the evolution of pyrolysis gases when during the baking process the binder is fluid(1). Also the filler particles may contain gross porosity which can be reduced by grinding before mixing and pressing. Micropores are formed parallel to the layer planes when, during cooling down from graphitization temperature, stresses are developed which at temperatures lower than 2000°C are relieved not by thermal creep but by the formation of the cleavage mentioned above. The micro-cracks are more pronounced in well graphitized than in poorly graphitized materials.

Porosity is fundamental relevance for the physical and chemical properties as well as irradiation behaviour. It was correlated with electrical resistivity, thermal conductivity, thermal expansion, strength, Young's modulus of elasticity and permeability. (2) Relationships exist between porosity, corrosion, fission product transport and adsorption.

Experiments were therefore carried out to apply various methods for measuring porosity and to investigate some factors which influence changes in porosity.

Experimental Considerations

Graphites heat treated at 2300°C, 2500°C, 2800°C and 3000°C were irradiated at temperatures between 1050°C and 1250°C in the DRAGON Reactor at Winfrith/England and a number of graphites of potential interest for in HTR applications were irradiated in the HFR Petten as part of the Joint DRAGON/ECN/EURATOM/KFA programme. The porosities were measured by applying impregnation methods (xylene, mercury) to determine open porosity, small angle x-ray scattering for the determination of the interpore spacing as an indication of the proportion of micropores and the quantitative image analyzer for the measurement of total macroporosity. For the measurement of open porosity using liquid infiltration, the samples were evacuated, impregnated with xylene and finally weighed to determine the increase in weight, Using the specific weight of the liquid, the pore volume can be calculated. The pore size distribution is commonly determined by using the mercury penetration method. Mercury is pressed stepwise into the open pores and under the assumption of cylindrical pores a mathematical pressure-to-pore diameter relation is used for determining pore sizes.

$$p \cdot r = 2\sigma\cos\theta \qquad (1)$$

p = pressure, r = radius of pores, σ surface tension, θ = limiting angle between mercury and specimen.

This method is valid for pore entrance diameters of more than 4 nm . One limitation for the application of this method is the danger of breaking the pore walls, especially after high fluence irradiation when the graphite becomes brittle.

By means of quantitative image analysis it is possible to indentify and measure pores which are so large that they cannot be measured by mercury porosimetry because of instantaneous penetration under atmospheric pressure. The upper boundary value for the pore size which can be measured by mercury porosimetry is in the range of a few µm, whilst quantitative image analysis is suitable for pore diameters up to several hundred µm. The essence of quantitative image analysis is that the classification of graphitic materials to be inspected is possible on the basis of the grey value contrast between pores (dark) and carbon (bright). Macroporosity is defined as total of all pores - open as well as closed - with diameters larger than 0.2 µm (3). The results obtained from optical analyses are area measurements.Because of the inhomogeneity, especially in coarse grain materials, the measurements taken at the surface of the ceramographic sections are not fully representative of the volume porosity. Another limitation is the assumption of spherical pores in the graphite which is not in fact the case. This theoretical problem is still under investigation. For small angle X-ray scattering (SAXS) measurements, an apparatus, consisting of a step scanning device, Cu-K$_\alpha$ radiation and a proportional counter with a discriminator and a teletype to measure an register the scattered X-ray intensity was used. With this equipment, pores of all shapes in a range of sizes between 1 and 100 nm with a tolerance of about 5% can be detected. The measured gap between high and low electron densities is a measure of the inter-pore spacing.

Results

Influence of graphitization temperature:

Fig. 1 shows that with increasing graphitization temperature the inter-pore spacing in the micropore region increases. The larger micropores result from the higher stresses which are built up during cooling down from the highest heat-treatment temperatures. This tendency can also be found in fig. 2 where the proportion of micro- and mesopores is greatest in the material graphitized at 3000°C. Though bulk density was only increased from 1.65 · cm^{-3} to 1.75 g cm^{-3} by increase in temperature from 2300°C to 3000°C, macroporosity and its distribution were considerably affected (fig. 2).

Influence of irradiation

The inter-pore spacing determined by small angle X-ray scattering was increased by irradiation at temperatures higher than 1000°C. This increase was the greater, the larger the pre-irradiation values of inter-pore spacing. This result is in agreement with TEM observations (4). Fig. 4 demonstrates that neutron irradiation causes a slight increase in macroporosity for pore diameters of 5 to 30 µm. The porosity consisting of still larger pores is reduced by irradiation in the case of the well graphitized sample. Fig. 5 shows the irradiation induced change in open porosity of gilsocarbon graphite measured by means of mercury porosimetry. Low fluence causes a decrease in porosity, but at high fluence, when the graphite has begun to swell, pores and a decrease around the smaller pores occurs. Two explanations are possible: 1)The generation of new pores and 2) breaking of the pore walls because of the high mercury pressure which must be applied to measure pores with very small entrance diameter.

References

(1) L.C.F. Blackman: Modern aspects of graphite technology, Chapter I: J.M. Hutcheon: Polycrystalline carbon and graphite, Academic Press, 1970
(2) J.M. Hutcheon, M.S.T. Price: 4th Conf. Carbon, 1960, 645

(3) W. Delle, K. Koizlik, H. Hoven, H. Uhlenbruck, E. Wallura: Proc. 5th Int. Carbon and Graphite Conf., Vol. I, 1978, 41
(4) E. Pollmann: Private Communication, 1979

Acknowledgements
This work has been carried out in the framework of the Project "Hochtemperaturreaktor-Brennstoff-Kreislauf" (High Temperature Reactor Fuel Cycle) that includes the partners Gelsenberg AG, Gesellschaft für Hochtemperaturreaktor-Technik mbH, Hochtemperaturreaktor-Brennelement GmbH, Hochtemperatur-Reaktorbau GmbH, *Kernforschungsanlage Jülich GmbH, Nukem* GmbH, Sigri Elektrographit GmbH, Ringsdorff-Werke GmbH and is financed from BMFT (Federal Ministry for Research and Technology) and the State of Nordrhein-Westfalen.

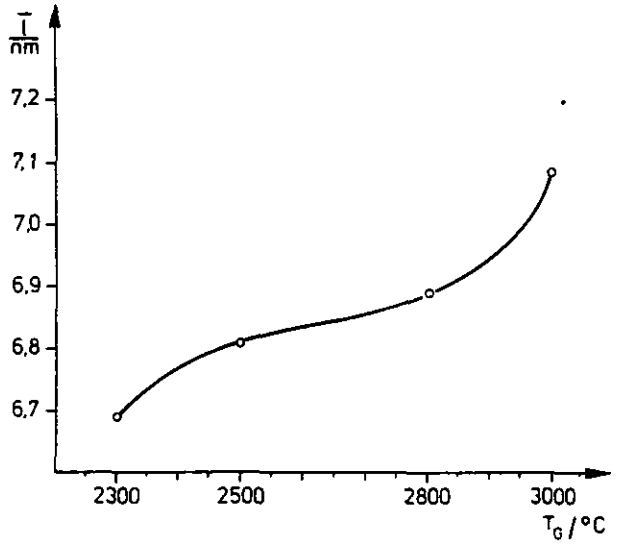

Fig. 1: Mean value of inter-pore spacing, $\bar{l}$, vs. graphitization temperature, T_G

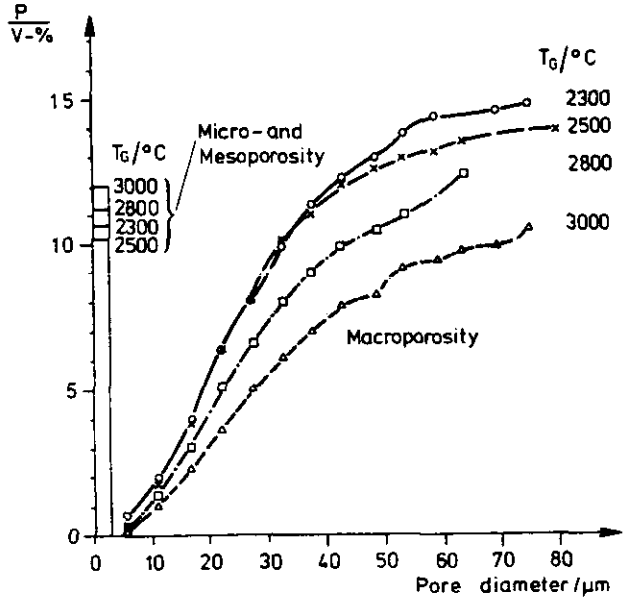

Fig. 2: Macropore size distribution of petroleum coke graphites of identical composition, but heat-treated at different temperatures, T_G

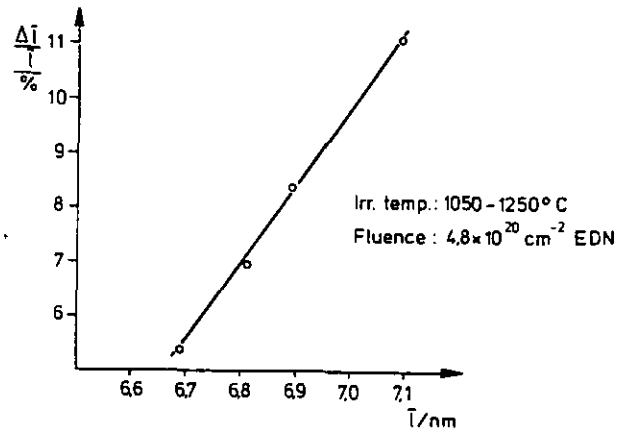

Fig. 3: Irradiation induced fractional change of mean value of inter-pores space, $\bar{l}$, vs. pre-irradiation value of $\bar{l}$

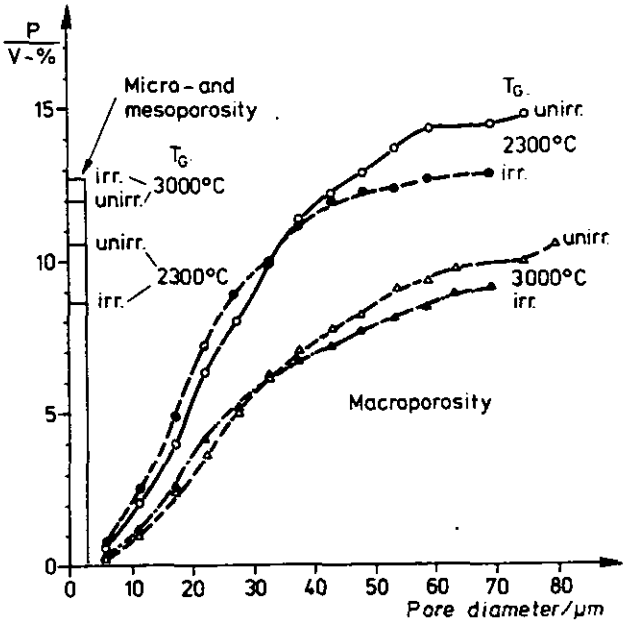

Fig. 4: Macropore size distribution before and after irradiation (4.8×10^{20} cm^{-2}EDN, 1050-1250°C) for petroleum coke graphites heat-treated (T_G) at 2300°C and 3000°C

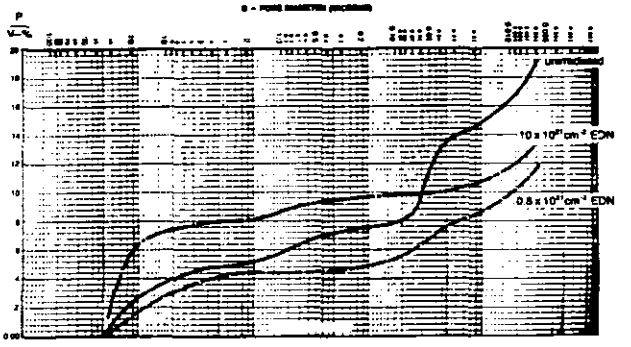

Fig. 5: Pore size distibution of gilsocarbon graphite before and after irradiation at 1000°C (mercury porosimetry)

BURN-OFF DEPENDENCE OF THE GRAPHITE CORROSION PROCESS UNDER IN-PORE DIFFUSION CONTROLLED CONDITIONS

R. Moormann, P. Ashworth

KFA Jülich, Institut for Nuclear Safety Research

Introduction

It is a well-known experimental fact that the reaction rates of graphite with corrosive gas mixtures in conditions of in-pore diffusion control increase with burn-off. The increase can be as much as an order of magnitude before a characteristic plateau is reached. This behaviour is of significance in the estimations of graphite corrosion related to High Temperature Reactors in two ways. Firstly, it is necassary to know the reaction rate distribution in the core and structural graphite at any particular time for the estimate of subsequent corrosion and secondly, because the strength loss of graphite is influenced by the corrosion profile and this profile is influenced by the burn-off dependence of the reaction rate, so this phenomenon is involved in strength loss calculations.

A survey of the literature together with some recent data is presented below

General Background

When graphite is corroded, structural changes occur; at lower burn-offs the accessible pore volume and the reactive graphite surface increase as carbon is removed and as blind pores are opened. At higher burn-off, the internal surface decreases as pore walls are removed.

In the chemical regime, or volume corrosion conditions, the reaction rate is influenced by burn-off only by changes in the the reactive surface area and therefore the reaction rate should increase to a maximum at medium burn-off values and then diminish to zero at total burn-off. Reaction rate measurements as a function of burn-off up to burn-off values of 30% were carried out by Tyler et al. /1/ for the graphite/oxygen reaction in the chemical regime. A maximum reaction rate was found at burn-off values near 25%. Walker et al. /2/ and Wicke et al. /4/ measured the internal carbon surface area as a function of burn-off and found a maximum at burn-off values of 40%. A theoretical approach to the calculation of the active surface area as a function of burn-off has been made by Stark and Malinauskas /3/ for low burn-off values.

For the in-pore diffision controlled regime the relationship between reaction rate and burn-off is more complicated. The local changes in the graphite structure cause significant changes in the pore mass transport processes, reflected in a varying effective diffusion coefficient and time dependent concentration and corrosion profiles in the graphite.

For slab geometry, the corrosion process in these conditions can be described by the diffusion equation:

$$\varepsilon\left(\frac{\partial c}{\partial t}\right) = D_{eff}\cdot\left(\frac{\partial^2 c}{\partial x^2}\right) - RG_v \qquad (1)$$

Both the effective diffusion coefficient and the reactive surface area, which affects the rate constant, are functions of the local burn-off value in the graphite. Because the gas composition changes are relatively fast, a pseudosteady state condition is quickly attained and the explicit time dependence term may be dropped. However, the time dependence of the diffusion process and of the reaction rate with increasing burn-off lead to a set of differential equations for which analytical solutions are not generally possible. Moreover, moving boundary conditions are necessary to account for dimensional changes as carbon is removed from the original geometrical surface.

Current Status

In the following the theoretical and experimental work on the influence of burn-off on corrosion are reviewed. Most of the theoretical approaches are confined to first order reactions and the differences lie in the way in which the burn-off dependence of diffusion and rate are handled. Petersen /5/ used, firstly, a single pore model the diameter of which increased with corrosion and so affected the kinetic parameters. A second model involved randomly distributed and connected pores of average diameter and the comparison of theory and experiment for the CO_2/graphite reaction gave good agreement. Wen /6/ does not use any explicit pore model but assumes that $D_{eff} \sim \varepsilon^{2-3}$ and that the internal surface decreases linearly with increasing porosity. Solutions for other than first order reactions are reported. Hashimoto and Silveston /7/ used special assumptions for pore size growth, initiation of new pores etc. and one significant outcome was the apparent independence of the results on whether the effective diffusion coefficient was held constant or burn-off dependent.

Work on the H_2O/graphite reaction in the IPDR was carried out at the DRAGON Project for a range of materials and the final results were reported as part of the KFA Data Retrieval Program /8/. The objective was to establish the systematics of behaviour for a material in relatively inexpensive and rapid out-of-pile measurements at near-atmospheric pressures and to correlate the data for application to in-pile high pressure conditions.

Kinsey /9/ had shown that at temperatures well above the transition region, the corrosion profiles in two pieces of graphite at different pressures can be made the same by adjustment of the temperatures although the rate of development of the profile will not be the same. This equivalence can be expressed mathematically by representing the diffusion equations in dimensionless forms and this approach was extended to explain certain experimental observations. It was shown, for example, that the apparent activation energy E_A will change with burn-off, starting at $E_A^{CR}/2$ for near zero burn-offs, then increasing as the reaction rate increases with burn-off and finally decreasing when the burn-off plateau is reached. Therefore, the derivation of activation energies must be carried out with data for low burn-off.

A further step was to transform the differential equations to to a set of coordinates moving with the corrosion profile at a velocity given by the total corrosion rate (the sum of the rates of corrosion and erosion). From this analysis it was shown that a maximum factor of corrosion rate increase with burn-off existed given by:

$$F = \left\{\frac{(\lambda\mu)_{max}}{\lambda_o}\right\}^{0.5} \qquad (2)$$

and that an inverse correlation should exist be-

tween this factor and the initial reactivity.

The first data to be correlated were a series of measurements of the temperature coefficient of the graphite-water reaction for several reactor grade graphites in the temperature range 1000-1300°C. From the rate versus burn-off curves thus obtained for each sample a value of the corrosion rate at very low burn-off (1 mg/cm^2) was interpolated. This was repeated for a new batch of specimens at each temperature.

The mean and standard deviation of the derived activation energy was 170±4 KJ·mol^{-1}. The second fact to be established was that erosion gave a negligable addition to the total weight loss. Measurements were carried out using a flow of argon up the central 6 mm bore channel of graphite specimens after successive periods of corrosion. The same Reynolds number for corrosion and erosion tests was used.

Little erosion was measured until a weight loss of 60 mg/cm^2 was reached where there was a sharp change to a new constant rate of erosion (4% of the total weight loss). This corresponded closely to the point at which a constant rate of corrosion had been established.

The dependence of the temperature coefficient on burn-off was then determined and the expective increase with burn-off followed by a decrease to the initial value when the rate/burn-off plateau is reached is shown in Fig.1.

Finally the strong inverse correlation found between the factor of increase of the rate of oxidation with burn-off and the initial reactivity is shown in Fig. 2 corresponding to prediction.

Code Development

A model similar to that used by Kinsey for solving the diffusion-corrosion equation has been developed as a part of a general graphite corrosion code for HTR's. Relationships for the burn-off dependence of the reactive surface and of the effective diffusion coefficient have been introduced, the latter being expressed by the equation:

$$\lambda = \lambda_o + (1-\lambda_o)\ B^2 \qquad (3)$$

Calculations are done assuming λ values of 0.01 for uncorroded graphite. The increase factor of rate with burn-off for a reaction order of 1 is in line with the upper limit value (2) predicted by the theory. Corrosion profiles have been developed using this code and correspond with measured data /10/. All shapes are qualitatively the same, and an example is shown in Fig. 3. At low burn-off, the shape is exponential; at higher burn-off, a region with small density gradients near the surface exists and the graphite near the surface is characterized by a low reactive surface area and a high value of D_{eff}, so that the corrosion rate is low. This profile, having been established, then moves with nearly unchanged shape into the graphite as burn-off proceeds.

Conclusion

A semi-empirical approach to the solution of the diffusion and reaction equations has enabled the corrosion data obtained at different pressures and temperatures to be correlated, an upper limit to the increase of corrosion with burn-off to be set and the form of the density profiles and the change of activation energy with burn-off to be predicted.

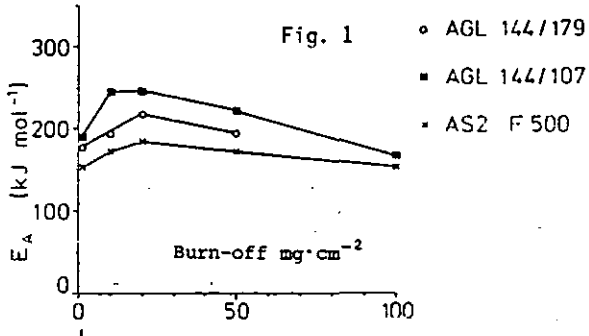

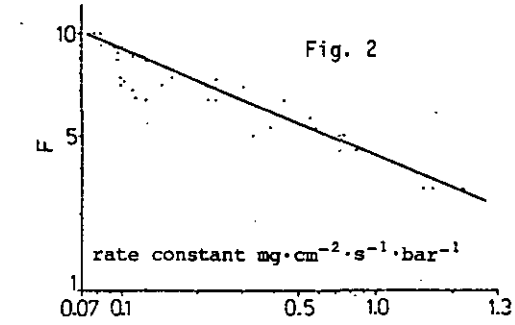

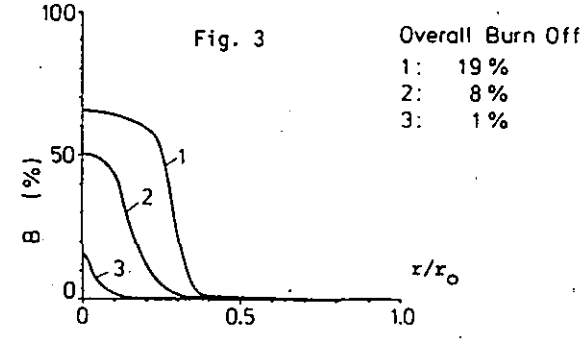

Literature

/ 1/ R.J. Tyler, H.J. Wouterlood, M.F.R. Mulcahy: Carbon 14 (1976) 271

/ 2/ P.L. Walker: 5th London Int. Conf. Carbon Graphite (1978) 427

/ 3/ W.A. Stark, A.P. Malinauskas: Los Alamos Rep. LA-UR-77-1956 (1977)

/ 4/ E. Wicke: 5th Symp. on Combustion (1955) 245

/ 5/ E.E. Petersen: AIChE J. 3 (1957) 443

/ 6/ C.Y. Wen: Ind. Eng. Chem. 60 (1968) 34

/ 7/ K. Hashimoto, P.L.Silveston: AIChE J. 19 (1973) 268

/ 8/ V.J. Wilkinson, R. Salvarani, D.V. Kinsey, F.P.O. Ashworth: KFA/DRAGON Data Retrieval Program; Final Status Report Meeting, April (1976)

/ 9/ D. Kinsey, J. Wilkinson: DRAGON Project Techn. Note 247 (1972)

/10/ G.H. Helsby, M.R. Everett: DRAGON Project Report 566 (1968)

List of Symbols

B	burn-off mg·cm^{-2}
E_A/E_A^{CR}	activation energy in IPDR /CR KJ·mol^{-1}
F	rate increase factor with burn-off
IPDR	in pore diffusion controlled regime
RG_V	rate in chemical regime mg·cm^{-3}·s^{-1}
ε	porosity
λ	D_{eff}/D
μ	reaction surface area related to B=0

THE DEPENDENCE OF THE CORROSION RATE OF THE A3-MATRIX/OXYGEN REACTION ON OXYGEN PARTIAL PRESSURE

R. Moormann, W. Katscher, H.K. Hinssen

KFA Jülich, Institut for Nuclear Safety Research

Introduction

For calculations of graphite corrosion caused by accidental air ingress into High Temperatur Reactors it is necessary to know the kinetic parameters of the graphite/oxygen reaction (especially under in-pore-diffusion controlled conditions); this paper deals with the evaluation of the partial pressure dependence of the A3-matrix/oxygen-reaction rate. The contents of A3-3-matrix material are 72% natural graphite, 18% petroleum coke and 10% Phenol resin binder; it is heat treated at 1950°C. A3-matrix material is used in manufacturing of the fuel elements of the german pebble bed reactor. To describe the partial pressure dependence of the graphite/steam- or of the graphite/CO_2-reaction rate under volume corrosion conditions, normally a Hinshelwood-Langmuir-equation is used /1,2/. In contrast, for the graphite/oxygen-reaction, the partial pressure dependence of the reaction rate is not well known /3/, but a Hinshelwood-Langmuir like equation should be valid for the graphite/oxygen reaction,too, although the reaction mechanism is complicated by the existence of a stable carbon/oxygen-complex at lower temperatures /4,5/. In the following experimental data, measured in IPDR, are fitted to an expression, derived from a Hinshelwood-Langmuir like equation. The corresponding reaction rate equation, valid for volume corrosion regime, is also evaluated.

Experimental

The experimental facilities for our measurements of the graphite/oxygen-reaction are described in detail in /3/; our measurements on A3-matrix-material cover an oxygen partial pressure regime of $2\cdot10^{-3}$ to 0.15 bar and a temperature regime of 700° to 900° °C . The total pressure was 1.5 bar ; the inert gas used was Helium. All measurements are done in IPDR.

Theoretical Background

In concordance with our experimental results /3/, we assume, that the reaction products CO and CO_2 do not strongly inhibit the oxygen/graphite reaction; then,a Hinshelwood-Langmuir-equation

$$RG_V = \frac{k_v \cdot P_{O_2}}{1+k_1 \cdot P_{O_2}} \qquad (1)$$

should be valid for volume corrosion conditions. The solution of the following equation (infinite slab geometry under stationary conditions):

$$D_{eff} \cdot \left(\frac{\partial^2 P_{O_2}}{\partial x^2} \right) \cdot \frac{1}{RT} = \frac{k_v \cdot P_{O_2}}{1+k_1 \cdot P_{O_2}} \qquad (2)$$

gives the reaction rate in IPDR. With

$$RG_F = - D_{eff} \cdot \left(\frac{\partial P_{O_2}}{\partial x} \right)_{SURFACE} \cdot \frac{1}{RT} \qquad (3)$$

and using the boundary value condition:

$$P_{O_2} = 0, \quad \left(\frac{\partial P_{O_2}}{\partial x} \right) = 0 \qquad x \to \infty$$

the following solution is obtained by analytical methods:

$$RG_F = \left\{ \frac{2\, k_v D_{eff}}{RT} \left[\frac{P_{O_2}}{k_1} - \frac{1}{k_1^2} \cdot \ln\left(1+k_1 P_{O_2}\right) \right] \right\}^{0.5} \qquad (4)$$

This equation is not very suitable for fitting of experimental data, but this solution can be approximated without large error (at maximum 5%) by a simpler equation like

$$RG_F = \frac{a_1 \cdot P_{O_2}}{\left(1+a_2 \cdot P_{O_2}\right)^{0.5}} \qquad (5)$$

with $a_1 = \left(k_v D_{eff}/RT\right)^{0.5}$ and $a_2 = k_1/2$ (equation (5) gives the best least square fit of all equations (7) in the range of $0.2<l<1.5$). The apparent reaction order is calculated from equation (5) to:

$$m = \frac{1 + 0.5 \cdot a_2 \cdot P_{O_2}}{1 + a_2 \cdot P_{O_2}} \qquad (6)$$

Similiar to the rate constants k_v and k_1, the constants of equation (6)should have an Arrhenius-like temperatur dependence. In this considerations, the burn-off dependence of the reaction rate is not introduced, but it is shown in another paper /6/ that the increase factor of the reaction rate with burn-off under IPDR-conditions is nearly the same for all temperatures when the reaction order is held constant. Considering only reaction conditions with fully established corrosion profile, it is valid as a first approximation to handle this burn-off-dependence as a multiplicative factor in equation (5).

Evaluation of experimental data

From experiments, we get the reaction rate RG_F and the apparent reaction order m, both in a discrete partial pressure range at a definite temperature. Using equation (6) we calculated the values of a_2 from data of our experiments described in /3/ and some additional experiments done by other authors /7/ and us; the evaluation method gives large errors for apparent reaction orders near to 0.5 or 1.0; therefore, the data apart from a range of $0.6 \le m \le 0.95$ are not used in this calculation; in the next step we calculated the constant a_1 using equation (5).

The Arrhenius like temperature dependence of the constant a_2 calculated in this way holds only for nearly the same partial pressure range of oxygen; higher partial pressures give lower a_2-values and reverse; this means, that (under isothermal conditions) the dependence of the apparent reaction order from partial pressure is less then given by equation (5). Introducing an additional parameter l in equation (5), which controlles the inclination of the $RG_F = f(P_{O_2})$-curves, leads to the following rate equation in IPDR:

$$RG_F = \frac{a_1 \cdot P_{O_2}}{\left(1+(a_2 \cdot P_{O_2})^l\right)^{\frac{0.5}{l}}} \qquad (7)$$

The apparent reaction order is then given by:

$$m = \frac{1+0.5(a_2 \cdot P_{O_2})^1}{1+(a_2 \cdot P_{O_2})^1} \qquad (8)$$

and for the corresponding equation under volume corrosion conditions holds:

$$RG_V = \frac{k_v \cdot P_{O_2}}{(1+(k_1 \cdot P_{O_2})^1)^{1/1}} \qquad (9)$$

A sucessfull fit for all experimental data is available for l=0.4 instead of l=1.0. The Arrhenius-Plot is shown in figure I;using the reaction rate data published in /3/, the overall-activation-energy of $1.17 \cdot 10^5$ J·mol^{-1} and a rate increase-factor with burn-off of 4.0 /3/, we get the following rate equation for IPDR on uncorroded A3-matrix-material:

$$RG_F = \frac{7 \cdot 10^4 \, e^{-110000/RT} \cdot P_{O_2}}{(1+(5.5 \cdot 10^{-9} \cdot e^{180000/RT} \cdot P_{O_2})^{0.4})^{1.25}} \cdot \frac{1.5}{P_{GES}} \qquad (10)$$

For the calculation of the corresponding volume corrosion kinetic data, the knowledge of the diffusion coefficient ratio $\lambda = D_{eff}/D$ is necessary; for A3-Matrix material this ratio is not published, but the commonly used reactor graphitic materials have λ-values of ~0.01 /8/;using this value and a gas-diffusion coefficient of 4.1 cm^2·sec^{-1} for oxygen/helium mixtures at 800 °C and 1.5 bar (calculated by Chapman-Enskog-theory), the following rate for uncorroded A3-material under volume corrosion conditions

$$RG_V = \frac{9 \cdot 10^9 \cdot e^{-220000/RT} \cdot P_{O_2}}{(1+(1.1 \cdot 10^{-8} \cdot e^{180000/RT} \cdot P_{O_2})^{0.4})^{2.5}} \qquad (11)$$

is calculated. It is seen from equations (10) and (11), that the overall activation energies depend strongly on the reaction order. This could be one cause of the large discrepancies for activation energies, found in literature in the case of the oxygen/graphite reaction.

In the second figure, the volume corrosion rate equations (1) and (9) with l=0.4 are compared; dimensionless coordinates $RG^* = RG/k_1 \cdot k_V$ and $P^* = P/k_1$ are used. This figure shows,that the transition range between the reaction orders 1 and 0 is larger in the case of equation (1).

Summary

A rate equation for the IPDR has been developed from Hinshelwood-Langmuir kinetics for volume corrosion. The best fit to the experimental data from A3-matrix/oxygen IPDR reactions was found, when a modified Hinshelwood-Langmuir-equation was used. The modification provides a broader transition range between the regimes of reaction order 1 and 0. The fitted IPDR rate equation was then re-transformed to the volume corrosion regime.

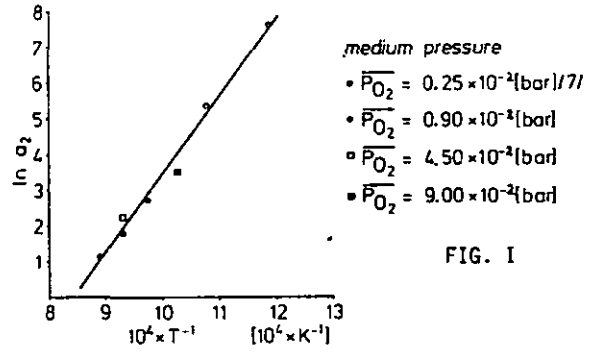

FIG. I

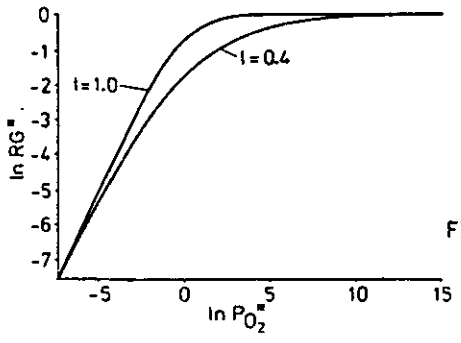

FIG. II

Literature

/1/ R.D. Burnette, C. Velasquez, G. Hightower, K. Koyama: 13th Bienn.Conf.Carbon (1977) 429

/2/ E. Wicke et al.: Dragon Project Report 391 (1965)

/3/ R. Moormann, J. Anhalt, H.K. Hinssen, P. Ashworth, W. Katscher: 5th London Int.Conf.Carbon Graphite (1978)108

/4/ H. Marsh, D.W. Taylor: 13th Bienn.Conf.Carbon (1977) 132

/5/ F.J. Vastola, P.J. Hart, P.L. Walker: Carbon 2 (1964) 65

/6/ R. Moormann, P. Ashworth: this conference

/7/ H. Jauer, P. Kubaschewski, H. Werthmann: CSNI-Spec.Meeting on HTGR Safety (1975)

/8/ R.T. Yang, R.T. Liu, M. Steinberg: Ind.Eng. Chem.Fund. 16 (1977) 486

List of symbols

D	gas diffusion coefficient cm^2·sec^{-1}
D_{eff}	effective diffusion coefficient cm^2·sec^{-1}
IPDR	in-pore diffusion controlled regime
P_{O_2}	oxygen partial pressure bar
P_{GES}	total pressure bar
RG_V	volume corrosion rate mg·cm^{-3}·sec^{-1}
RG_F	surface corrosion rate mg·cm^{-2}·sec^{-1}

THE STRENGTH OF REACTOR GRAPHITE AS PORTRAYED BY FRACTURE MECHANICAL DATA

M. Rödig, G. Kleist, H. Nickel
Kernforschungsanlage Jülich GmbH
D-5170 Jülich
Federal Republic of Germany

1. Introduction

The strength of graphite is generally characterized by its uniaxial ultimate tensile stress (UTS) and its modulus of rupture (MOR). Since graphite is referred to as a brittle material it seems reasonable to try the fracture mechanical approach in order to describe the resistance of reactor graphites to brittle failure. It was expected that by this means, additional information on the general fracture behaviour of graphite could be attained. The value of fracture toughness itself is needed in order to obtain an estimate of the fracture resistance of slottet reflector blocks being considered for eventual use in pebble bed HTR (1).

2. Experimental Details

The investigated material is the extruded pitch-coke graphite ASR-2E from Sigri Elektrographit GmbH. This graphite is a candidate for the outer reflector of the pebble bed HTR. For comparison, some experiments were performed with the nearly isotropic fine grain graphite EK 88 from the company Ringsdorff Werke. Some characteristic data of both graphites are listed in table 1.

The fracture mechanic tests were performed with CT-(compact tension) specimens (Fig. 1) according to ASTM-E399 (2). The specimens were loaded under strain control which approximates best the loading conditions for graphite in the reactor.

Stress intensity factors are calculated from

$$K_I = \frac{P}{b \cdot d} \sqrt{a} \cdot f(a/b)$$

where P is the load, a is the crack length, and b, d, f(a/b) are geometric parameters (see Fig.1). The initial cracks were saw cuts of 0.3 mm width.

In the case of ASR-2E crack-propagation started before the maximum of the load displacement curve was reached. Crack onset was detected by an electrical potential method. Stress intensity factors were calculated for both the load at crack onset and the maximum load. They are called K_0 and K_{max} respectively, according to normal nomenclature.

Acoustic emission techniques were applied to get additional information on the fracture process.

3. Results

The critical stress intensity factors K_0 and K_{max} were determined in all experiments. In addition, for some sets of specimens the critical J-integral J_0 (which is twice the initial specific surface energy γ_i) and the work of fracture γ_F were calculated. Table 2 lists the reference values of these parameters for both graphites in the case of the CT 30 mm specimen with a relative initial crack length of a/b = 0.5. It should be pointed out that for the fine grain graphite K_0 and K_{max} are identical.

It was found that the above mentioned data are dependent on the special position in a graphite block, on the production lot, on the orientation with regard to the pressing direction, on the density, on geometric parameters such as specimen volume and crack length, and further, on mechanical preloading.

As may be expected, the fracture toughness increases with increasing material density.

Fig. 2 shows the "volume effect", i.e. the increase of the critical stress intensity factors K_0 and K_{max} with specimen size. This has been discussed in some detail elsewhere (3). Another expression of the volume effect is the decrease of fracture toughness with increasing initial crack length. This may be understood by considering that a larger initial crack length means a smaller specimen ligament.

The equivalent volume effect was also found in measurements of the critical J-integral for ASR-2E with CT 10mm and CT 30 mm specimens (4).

The "preloading effect" is observed when one specimen with initial crack length a_0 is repeatedly loaded beyond maximum load: Then a subcritical crack growth Δa_1 is found resulting in the new crack length $a_1 = a_0 + \Delta a_1$. After unloading the following test starts from the crack length a_1 and gives another crack growth Δa_2 etc. Fig. 3 shows the increase of the stress intensity factors K_0 and K_{max} for two CT 30 mm specimens made of ASR-2E with different initial crack lengths a_0/b in a multiple loading experiment as a function of growing dimensionless crack length a/b.

With acoustic emission it was possible to get additional information on the distribution of energy dissipating processes in the specimen, which was helpful in the interpretation of the volume effect (3). Further it was possible with this technique to detect the onset of crack propagation (4).

4. Discussion

When our fracture mechanical investigations on reactor graphite were started it was not expected that fracture toughness would depend on specimen size since a plastic zone like in metals does not exist in brittle materials like graphite. The observed volume effect allows, however, the conclusion, that cracks in large graphite blocks are less dangerous than it might be expected from the testing of small specimens. This is clearly

in benefit of compact reflector blocks in operation in the HTR. The volume effect is explained by the increase of the portion of dissipated energy with increasing specimen dimensions.

Another surprising result is the fact, that the fracture toughness of the fine grain graphite with its rather high tensile strength is not significantly higher than that of the coarse grained ASR-2E. The difference in fracture toughness of both materials decreases the more the specimen volume is increased (Fig. 2). It may be expected that for even larger specimens the coarse grain reactor graphite will exceed the "high strength" material in a fracture mechanical sense. This is also expressed by the higher effective fracture energy for ASR-2E.

The experiments show that in the case of fine grain material, the crack once started can only be stopped by load reduction. For the coarse grain graphite, however, after crack onset the load can even be increased, since the crack-tip is released by parallel cracks and the formation of a tortuous crack path. By these effects the increase of the critical stress intensity factors K_o and K_{max} in multiple loading experiments with the coarse grain graphite can be explained.

From the fact, that both graphites show similar values of fracture toughness and from the observed crack arrest in the case of the coarse grain graphite, it may be concluded that from the fracture mechanical point of view a fine grain graphite has no essential advantage over a coarse grain material.

5. Acknowledgement

This work is being conducted within the frame work of the project "Hochtemperaturreaktor-Brennstoffkreislauf" (High Temperature Reactor Fuel Cycle) which contains the partners Gelsenberg AG, GHT GmbH, Hobeg mbH, HRB GmbH, KFA GmbH, Nukem GmbH, Sigri GmbH, Ringsdorff-Werke GmbH, and is financed by the Federal Ministry for Research and Technology and the state Northrhine-Westfalia.

6. References

(1) H. Cords, J. Mönch, R. Zimmermann: KFA Jülich internal report. IRW-IB-2/79, 1979.
(2) ASTM-E399, ASTM Book of Standard Vol. 31, Philadelphia 1973.
(3) M. Rödig, G. Kleist, H. Nickel: Fifth London International Conference on Carbon and Graphite, London, Sept. 18-22, 1978, proceedings, p. 51.
(4) M. Rödig, G. Kleist, H. Nickel: "Bestimmung des kritischen J-Integrals für einen Reaktorgraphit", Jül-1482, 1978.

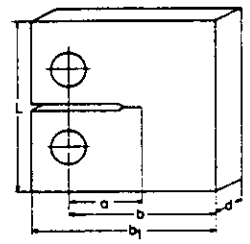

Fig. 1: CT-specimen

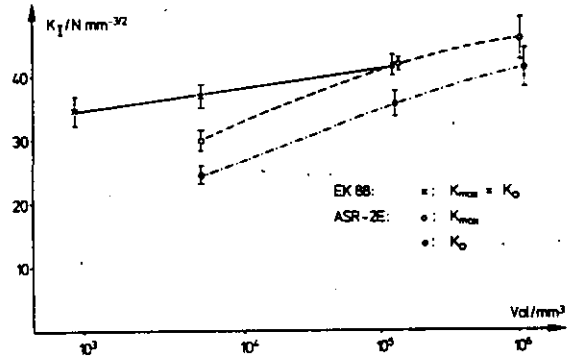

Fig. 2: Volume Influence on K_o and K_{max}

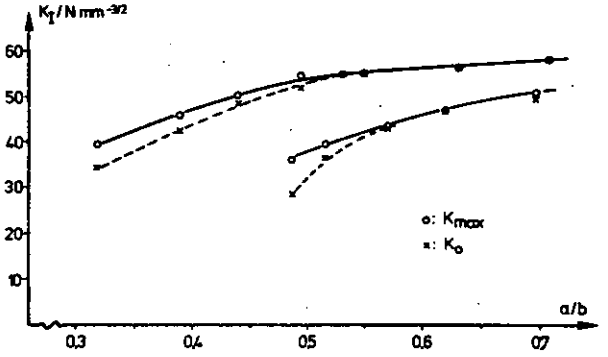

Fig. 3: Multiple Loading Experiments

		ASR-2E	EK 88
max. grain size/mm		1	0.05
apparent density/g cm^{-3}		1.76	1.85
Young's modulus/GPa	∥	10.3	12
	⊥	8.3	
tensile strength/MPa	∥	12.8	39
	⊥	11.3	
bending strength/MPa	∥	22.6	50
	⊥	17.7	

Table 1

	ASR-2E	EK 88
K_o/N mm$^{-3/2}$	42	42
K_{max}/N mm$^{-3/2}$	35	
J_o/N mm^{-1}	0.20	0.19
γ_F/N mm^{-1}	0.21	0.08

Table 2